Journal of Mines, Metals and Fuels, *72(1): 13-35; 2024. DOI: 10.18311/jmmf/2024/36131*

Print ISSN : 0022-2755

Journal of Mines, Metals and Fuels

Contents available at: *www.informaticsjournals.com/index.php/jmmf*

Investigation and Optimization on Parameters of Gas Additive Powder Mixed Near Dry –EDM (GAPMND-EDM) by using Taguchi based- Grey Relational Optimization

Ajit and Sanjay Sundriyal*

Department of Mechanical Engineering, Lingaya's Vidyapeeth, Faridabad , Haryana, 121001, India; ss95576@gmail.com

Abstract

The Gas Additive Powder Mix near Dry Electric Discharge Machining (GAPMND-EDM) serves a manufacturing purpose, specifically for cutting hard materials. This involves the removal of material from a workpiece via fusion, ablation, and evaporation caused by the heat energy generated through electric sparks during energy supply. The process offers several advantages in terms of performance and characteristics. This research project aims to optimize key process parameters, including material removal rate, surface roughness, residual stresses, and microhardness. The study employs a methodology that combines the standard deviation-based objective weighting method with GRA (Gray Relational Analysis) optimization to enhance the hybrid GAPMND-EDM process when applied to EN-31 material. Experimental runs were conducted to evaluate the impact of various input factors, such as pulse-on time, discharge current, dielectric fluid pressure, and metallic powder concentration. The taguchi-based GRA method was utilized for this purpose, and the experimental design followed an L-27 orthogonal array with the assistance of Minitab-19 software. A total of 27 experiments were performed, encompassing diverse combinations of process parameters. Subsequently, an ANOVA (Analysis of Variance) was executed to analyze the influence of pulse-on time, discharge current, dielectric fluid pressure, and metallic powder concentration on Material Removal Rate (MRR), Surface Roughness (SR), Residual Stress (RS), and Microhardness (MH). The result shows the optimal combination of parameters, denoted as A2B2C2D1, was identified as the preferred configuration.

Keywords: *Dry Air, GAPMND-EDM, Gas Additive, MRR, Metallic Powder, Residual Stress, Surface Finish*

1.0 Introduction

EDM, or electrical discharge machining, is a non-traditional method used for cutting materials and creating a variety of shapes and sizes for different applications. Various forms of EDM exist to enhance machining characteristics, such as increased material removal and improved quality of machined products. Near-Dry Machining (NDM) involves minimal lubrication or the application of a mist directly to the work surface. This innovative approach serves as an alternative to traditional coolant techniques with high pressure, aiming to reduce the consumption of Metal-Working Fluids (MWFs) and their associated costs. In Near Dry EDM (ND-EDM), the cooling medium consists of a mist made up of tiny droplets or aerosol, which is a mixture of oil and air. Here, "mist" refers to solid particles suspended in liquid or air. The concept of near-dry machining was first applied to

*Author for correspondence

EDM machines in 1981, prompting further exploration into using mist and various gases like argon and nitrogen as dielectric mixtures[1]. A study examined the impact of introducing graphite powder into kerosene on the breakdown voltage in Powder-Mixed EDM (PM-EDM)[2]. It was observed that specific concentrations of powder, such as graphite and silicon, when mixed with the dielectric fluid, resulted in exceptionally smooth surfaces due to the distribution of sparks in the spark gap[3]. Adding metallic powders to the dielectric fluid was found to increase Material Removal Rate (MRR) and decrease Tool Wear Rate (TWR). An effort was made to determine the optimal output parameters for PM-EDM, and the research demonstrated that setting output parameters at their optimum levels in PM-EDM resulted in a lower surface finish value and a higher MRR[4]. The investigation explored the impact of varying concentrations of graphite powder on the machining of H-11 die steel, specifically analyzing residual stress, tool wear rate, and material removal as key output parameters. The findings revealed that the addition of 6 g/l of graphite powder enhanced material removal, improved surface finishing (Ra), and Reduced Tool Wear (TWR)[5]. Another inquiry delved into different dielectrics in PM-EDM, showcasing that the HOPs (High Oil Pressure) study effectively reduced machining costs and dielectric damage while also mitigating environmental risks compared to traditional EDM methods[6]. Furthermore, the thermal aspects of PM-NDEDM were elucidated, exploring the influence of individual process parameters on Material Removal Rate (MRR)[7-9]. In PMEDM, optimization of plasma channel features was conducted, revealing significantly greater stability compared to traditional EDM when using a mixture of conductive metallic powder and oil. This stability was attributed to the compression of the plasma within PM-EDM, facilitated by an electric bridge formed by particles of conductive metallic powder in the EDM oil[10]. The research extended to the machining of titanium alloy (Ti–6Al–4V) workpieces using electrical discharge machining. The evaluation focused on parameters such as tool wear, material removal rate, and the quality of the machined surface finish. Topographical features and surface morphology were examined to provide a comprehensive understanding[11]. The impact of silicon carbon powder concentration on the surface topography, component deposition, and subsurface structures during Powder Mixed Electrical Discharge Machining (PMEDM) of Ti-6Al-4V-ELI material was explored. The results revealed that a higher concentration of suspended particles in the dielectric fluid promoted a particulate form of particle transfer mechanism[12]. The flushing or flooding mode plays a crucial role in the operation of the electrical discharge machine, and an improper approach can lead to irregular cutting and unfavorable machining processes[13]. Extensive research has also been conducted to understand the development of residual stress in machined samples. Models aimed at minimizing these residual stresses have been explored[14]. The investigation found that the subsurface of machined samples in EDM exhibited higher levels of residual stress compared to the surface, primarily due to the high roughness on the top surface. In the context of wire EDM, a parametric investigation into residual stresses was conducted using the Taguchi optimization method to reduce stresses in aluminum workpieces[15]. Additionally, the stress in AISI H13 tool steel exposed to the EDM process was evaluated using a combination of the nano-indentation technique and Raman spectroscopy[16]. The residual stress produced on an object made of high-carbon, high-chromium D2 tool steel was specifically examined using the X-ray method. This method was applied in a vibration-assisted hybrid EDM process to achieve optimal residual stress[17]. And conducted experiments on surface finish, tool wear rate, and MRR through a comparative analysis between PMND-EDM and ND-EDM, which stands for non-conventional electrical discharge machining. The findings revealed a lower tool wear rate in the PMND-EDM process compared to ND-EDM[18,19]. In the EDM process, SiC and Al powders are employed in dielectric oil. The introduction of metallic powder leads to an increase in the working gap between the workpiece and tool. This enlarged gap generates discrete sparks, facilitating efficient material removal and resulting in a smoother finishing surface[20]. Moreover, the study observed that the adoption of a minimal-quantity lubrication system not only enhances machining accuracy but also plays a role in preventing environmental pollution and safeguarding workers from potential hazards. The optimal use of metal-working fluids not only brings economic benefits but also aligns with environmentally friendly machining practices. While previous research has primarily focused on examining the Material Hardness (MH) of machined

components in GAPMND-EDM, this study aims to delve deeper into the complexities of GAPMND-EDM. After thoroughly reviewing existing literature, we have initiated a comprehensive exploration of GAPMND-EDM, examining factors such as Material Removal (MRR), Surface Roughness (SR), Residual Stress (RS), and Microhardness (MH). To facilitate this investigation, we designed a unique experimental setup that allows us to analyze the interaction among a three-phase dielectric pressure (solid, liquid, and gas), discharge current, pulse-on time, and metallic powder. Specifically, our experimental setup was tailored to investigate the impact of variations in metallic powder concentration on machining performance concerning the mentioned factors. Subsequently, we performed a comparative analysis of machining performance between GAPMND-EDM and PMND-EDM, drawing insights from the experimental results. While many researchers focus on optimizing Powder Mixed Near Dry EDM process parameters, to the best of our knowledge, there are no systematic studies integrating the standard deviation objective weighting method and the GRA-based Taguchi method for multi-objective optimization of the GAPMND-EDM process.Therefore, our study delves into the application of the standard deviation objective weighting method, an objective weighting technique, and the Grey Relational Analysis (GRA)-Taguchi-based method to address the multi-criteria optimization challenges in the gas additive powder mixed near-dry EDM process parameters for EN-31 die steel. This approach aims to enhance mechanical characteristics such as Material Removal (MRR), Surface Roughness (SR), Residual Stress (RS), and Microhardness (MH), ensuring consistent quality during GAPMND-EDM.

2.0 Experimental Methods

2.1 Materials

We selected an EN-31 (40 mm x 20 mm x 20 mm) workpiece for its outstanding hardness, impressive compressive strength, and resistance to abrasion. The exceptional wear resistance of this steel grade makes it well-suited for machining components, and it is widely utilized in the manufacturing industry. Additionally, we chose copper as the tool electrode for its superior thermal conductivity and other favorable attributes conducive to experimentation. Refer to Table 1 for the properties of the workpiece and Table 2 for the copper tool.

2.2 Design of Experiment

In this current study, input process parameters for the gas additive powder mixed near dry-EDM process were chosen to be Pulse on time, discharge current, dielectric fluid pressure, and powder concentration. These parameters were varied at different levels, as

Table 1. Chemical composition or structure and physical characteristics of workpiece -EN-31 material

Sr.	Chemical Characteristics		Physical Characteristics	
1	Element	Percentage	Thermal conductivity	44.5 W $m^{-1}K^{-1}$
2	Carbon	0.90-1.20	Hardness	63 HRC
3	Silicon	0.10-0.35	Yield stress	450 MPa
4	Manganese	0.30-0.75	Tensile strength	750 MPa
5	Sulphur	0.050	Density	7850 kg m^{-3}
6	Phosphorus	0.050	Melting point	1540 ^{0}C

Table 2. Physical and chemical characteristics of the copper tool

Sr.	Properties	Values
1	Atomic number	29
2	Atomic weight	63.546
3	Density(Kg m^{-3})	8960 Kg m^{-3}
4	Melting point	1083 ^{O}C
5	Boiling point	2567 ^{O}C
6	Thermal conductivity	385 Wm $^{-1}$ K $^{-1}$
7	Hardness	2.5-3 Mohs
8	Tensile strength	33.3 MPa
9	Bulk modulous	140 GPa

Table 3. Process parameters and their levels

GAPMNED-EDM process parameters	1	2	3	4
	Pulse on	**Discharge Current**	**Dielectric Fluid Pressure**	**Powder Concentration**
Level 1	35	4.00	0.2	4.00
Level 2	292.5	8.00	0.4	6.00
Level 3	550.00	12.00	0.6	8.00

Table 4. Different-2 conditions of dielectric fluid combination of experimentation

Conditions	1	2	3	4	5	6
Dielectric combination	Aluminium + Helium	Aluminium + Nitrogen	Zinc + Helium	Zinc + Nitrogen	Graphite + Helium	Graphite + Nitrogen
Dielectric oil: stabilizing agent: 4-6 % glycerol, Powder concentration 4, 6, 8 g/l, Flow meter of dielectric: 12 ml/min: Dielectric fluid pressure: 0.2 , 0.4 , 0.6 MPa						

outlined in Table 3, resulting in a total of 81 (3 × 3 × 3 × 3) potential combinations. However, utilizing the L-27 orthogonal array design, only 27 specific combinations were considered for sample development. This approach ensured that the outputs obtained were as reliable as if all 81 combinations had been individually taken into account, in accordance with the principles outlined in reference[27]. The experiment was conducted using the

Design Of Experiment (DOE) method in Minitab-19 software, incorporating the L-27 orthogonal array design, as detailed in Table 7.

2.3 Gas Additive Powder Mixed- NDEDM

The design and development of the latest and most

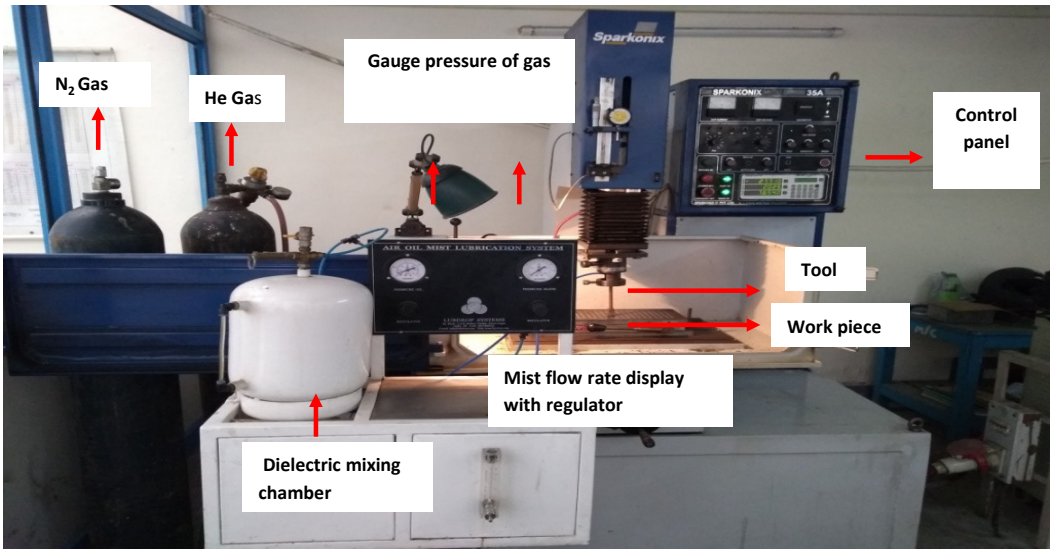

Figure 1. Setup for experimentations (GAPMND-EDM).

Table 5. Classification by parameters for gas additive powder mixed near dry (GAPMND) EDM

Parameters		Classification
1	Work piece	EN-31 (40 x 20 x20) (dimensions in mm)
2	Tool Electrode	Copper tool
3	Dielectric	Helium, N_2 +oil (LL-221) +metallic powder
4	Discharge Current	4A , 8A, 12A
5	Gap Voltage	30 V
6	Pulse On / Off	550 µs/35 µs
7	Polarity	+ve
8	Powder concentration	4,6,8 (g/l)
9	Flow meter of dielectric	12 ml/min
10	Air and oil Pressure	0.2 ,0.4 , 0.6 MPa
11	pressure gauge	Accuracy: (permissible error 0.05% of span)
12	Stabilizing agent	Glycerol (4-6 %)

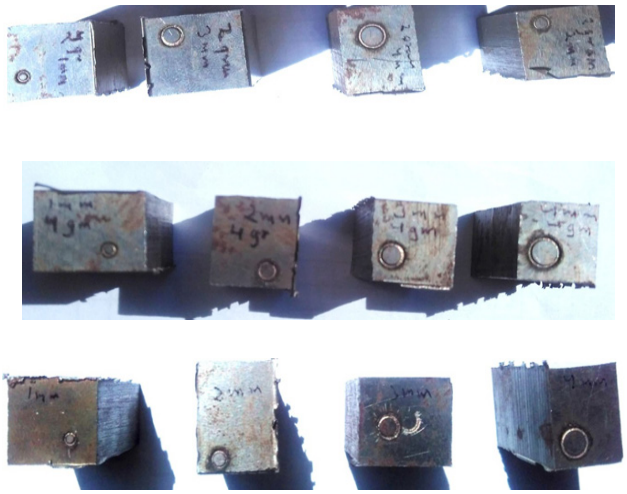

Figure 2. Machined samples (GAPMND-EDM).

advanced gas additive powder-mixed NDEDM setup were successfully completed. Figure 1 illustrates the experimental arrangement for GAPMND-EDM, which was crafted with minimal resource input, prioritizing environmental friendliness while achieving the characteristics of the required response. This innovative GAPMND-EDM setup employs a heterogeneous mixture comprising three phases- solid, liquid, and gas- as its medium of dielectric. The setup's panel incorporates various key components, including a dielectric chamber for mixing, a mist flow meter for a dielectric, manual regulators, and pressure gauges that play a crucial role in determining the working pressure of the dielectric medium.

3.0 Standard Deviation Objective Weighting Method

The standard deviation objective weighting method was utilized to determine the weight (w_j) of each criterion.

The Performance Defining Criteria (PDC) for all responses were established based on these weights. Initially, a decision matrix was defined, encompassing 27 experiments and four process parameters. Subsequently, by calculating the best and worst values for all process parameters, the decision matrix was normalized using Equation (1).

$$X_{ij}^{+} = \frac{X_{ij} - X_j^{\text{worst}}}{X_j^{\text{best}} - X_j^{\text{worst}}} \quad (1)$$

where X_{ij}^{+} represents the normalized value of the ith design on the jth response. By applying correlation and standard deviation coefficient (Minitab 19 software). After this, correlation and standard deviation coefficients were employed to evaluate information creation. Then, each criterion's weight (ξ_j) was calculated using Equation (2).

Based on the weight of responses, the Performance-Defining Criteria (PDC) was decided for all responses, as shown in Table 6.

$$\xi_j = \frac{c_j}{\sum_{k=1}^{m} c_j} \quad (2)$$

Where, $\xi_j \geq 0$ and $\sum_{k=1}^{m} c_j = 1$

Table 6. Performance Defining Criteria (PDCs)

SN	Performance-defining criteria (PDC)			Impact on PDC
	Response	Weight (ξ)	Designation	
1	Material removal rate	0.8	PDC-1	Higher the better
2	Surface roughness	0.1	PDC-2	Lower the better
3	Residual stress	0.1	PDC-3	Lower the better
4	Micro hardness	0.9	PDC-4	Higher the better

4.0 Hybrid Gray Relational Methodology

4.1 S/N Ratio

Categorizing characteristics, three signal-to-noise (SN) ratios are considered: lower-the-better, higher-the-better, and nominal-the-better. In this study, higher-the-better ratios are employed for the Material Removal Rate (MRR), Surface Roughness (SR), Residual Stress (RS), and Microhardness (MH). The expressions representing these approaches are outlined below.:
SN ratio for "lager is better"

$$SN_L = -10log(\frac{1}{n}\sum_{i=1}^{n}\frac{1}{y^{i^2}} \quad (3)$$

SN_s ratio for "Smaller is better"

$$SN_s = -10log\sum_{i=1}^{n} y^{i^2} \quad (4)$$

SN_n ratio for "nominal is better"

$$SN_n = 10\log 10\ (Square\,of\ mean\ /\ variance) \quad (5)$$

4.2 Normalisation of S/N Ratio

For larger the better for MRR , SR and RS and MH.

$$y_i^*(m) = \frac{y_i(m) - \min y_i(m)}{\max y_i(m) - \min y_i(m)} \quad (6)$$

For smaller, the better

$$y_i^*(m) = \frac{\max y_i(m) - y_i(m)}{\max y_i(m) - \min y_i(m)}. \quad (7)$$

For nominal, the better for

$$y_i^*(m) = \frac{1 - /y_i(m) - y_0 b(m)/}{\max y_i(m) - y_0 b(m)}. \quad (8)$$

Y*(m) and y_i(m) are the data preprocessing and comparability arrangements. M = 1, m = 2, m = 3, m = 4 for MRR, SR and RS and MH, I = 1, 2, 3, 27 for experiment no. 1 to 27.

4.3 Deviation Sequence

The deviation sequence can be represented as:

$$\Delta_{0i}(k) = \left|y_0^*(m) - y_k^*(m)\right| \quad (9)$$

4.4 Grey Relational Coefficient (GRC)

The connection among best with real normalized experimental value is expressed by GRC.

$$GRC = \hat{\imath}_i(k) = \frac{\Delta_{\min} + \hat{\imath}\,\Delta_{\max}}{\Delta_{0i}(\hat{k}) + \Delta_{\max}}. \quad (10)$$

4.5 Grey Relational Grade

It is determined by averaging the GRCs for every performance property. The overall calculation of multiple performance characteristics depends on grey relational grades.

$$\gamma_i = \frac{1}{n}\sum_{k=1}^{n}\xi_i(k) \quad (11)$$

5.0 Optimization using GRA Method

The experiments were carried out at room temperature following the face-centered composite design. Material Removal Rate (MRR), Surface Roughness (SR), Residual Stress, and Microhardness (MH) were computed from the load-displacement graphs for all 27 runs, and the results are depicted in Figures 4-7.

The Signal-to-Noise (S/N) ratio for Material Removal Rate (MRR), Surface Roughness (SR), residual stress, and Microhardness (MH) was determined using Equation (3) and is presented in Table 8. The normalized S/N ratio, considering Material Removal Rate (MRR), Surface Roughness (SR), Residual Stress, and Microhardness (MH), was calculated using Equation (6) and is detailed in Table 9. The deviation sequence for all experimental trials was computed using Equation (9) and is outlined in Table 10.

Table 7. Experiment results

	Factor 1	Factor 2	Factor 3	Factor 4	RI	R2	R3	R4
Run	A:Pulse on	B:Dis-charge Current	C:Dielectric Fluid Pressure	D:Powder Concen-tration	Material Removal Rate	Surface Rough-ness	Residual Stress	Micro Hardness
	µs	Ampere	%	g/l	Mg/min	µm	MPa	VHN
1	35	4	0.2	4	1.6	1.3	800	700.21
2	35	4	0.2	4	0.09	0.06	700	415.45
3	35	4	0.2	4	0.05	0.02	415	150.25
4	35	8	0.4	6	0.1	0.08	150	380.36
5	35	8	0.4	6	0.5	0.3	380	350.42
6	35	8	0.4	6	1.2	0.9	350	366.45
7	35	12	0.6	8	1.65	1.35	366	650.21
8	35	12	0.6	8	1.22	0.92	650	420.89
9	35	12	0.6	8	1.24	0.94	420	395.78
10	292.5	4	0.4	8	1.26	0.96	395	398.25
11	292.5	4	0.4	8	0.5	0.2	398	320.78
12	292.5	4	0.4	8	1.72	1.42	229	605.70
13	292.5	8	0.6	4	1.29	0.99	605	380.41
14	292.5	8	0.6	4	1.71	1.31	380	500.45
15	292.5	8	0.6	4	0.39	0.19	500	320.08
16	292.5	12	0.2	6	1.3	1	320	360.25
17	292.5	12	0.2	6	1.7	1.4	360	600.07
18	292.5	12	0.2	6	1.3	1.02	600	295.26
19	550	4	0.6	6	0.44	0.14	295	300.22
20	550	4	0.6	6	0.41	0.11	300	309.17
21	550	4	0.6	6	1.04	0.74	309	349.79
22	550	8	0.2	8	1.74	1.34	349	610.44
23	550	8	0.2	8	1.39	1.09	610	419.38
24	550	8	0.2	8	0.4	0.1	419	220.11
25	550	12	0.4	4	0.39	0.09	220	251
26	550	12	0.4	4	1.75	1.45	251	605
27	550	12	0.4	4	2.3	2.1	605	821.32

Table 8. S/N ratio

Run	A:Pulse on	B:Discharge Current	C:Dielectric Fluid Pressure	D:Powder Concentration	S/N Ratio MRR	S/N Ratio Surface Roughness	S/N Ratio Residual stress	S/N Ratio Micro-Hardness
	µs	Ampere	%	g/l				
1	35	4	0.2	4	7.234557	-2.27887	-58.0618	-56.9046
2	35	4	0.2	4	4.0824	24.43697	-56.902	-52.3704
3	35	4	0.2	4	-20.9151	33.9794	-52.361	-43.5363
4	35	8	0.4	6	-26.0206	21.9382	-43.5218	-51.6039
5	35	8	0.4	6	-20	10.45757	-51.5957	-50.8918
6	35	8	0.4	6	-6.0206	0.91515	-50.8814	-51.2803
7	35	12	0.6	8	1.583625	-2.60668	-51.2696	-56.2611
8	35	12	0.6	8	4.349679	0.724243	-56.2583	-52.4834
9	35	12	0.6	8	1.727197	0.537443	-52.465	-51.9491
10	292.5	4	0.4	8	1.868434	0.354575	-51.9319	-52.0031
11	292.5	4	0.4	8	2.007411	13.9794	-51.9977	-50.1241
12	292.5	4	0.4	8	-6.0206	-3.04577	-50.103	-55.6452
13	292.5	8	0.6	4	4.710569	0.087296	-55.6351	-51.605
14	292.5	8	0.6	4	2.211794	-2.34543	-51.5957	-53.9872
15	292.5	8	0.6	4	4.659922	14.42493	-53.9794	-50.1052
16	292.5	12	0.2	6	-8.17871	0	-50.103	-51.1321
17	292.5	12	0.2	6	2.278867	-2.92256	-51.1261	-55.564
18	292.5	12	0.2	6	4.608978	-0.172	-55.563	-49.4041
19	550	4	0.6	6	2.278867	17.07744	-49.3964	-49.5488
20	550	4	0.6	6	-7.13095	19.17215	-49.5424	-49.8039
21	550	4	0.6	6	-7.74432	2.615366	-49.7992	-50.8761
22	550	8	0.2	8	0.340667	-2.5421	-50.8565	-55.7129
23	550	8	0.2	8	4.810985	-0.74853	-55.7066	-52.4522
24	550	8	0.2	8	2.860296	20	-52.4443	-46.8528
25	550	12	0.4	4	-7.9588	20.91515	-46.8485	-47.9935
26	550	12	0.4	4	-8.17871	-3.22736	-47.9935	-55.6351
27	550	12	0.4	4	4.860761	-6.44439	-55.6351	-58.0618

Table 9. Normalise signal-to-noise ratio of response

Run	A:Pulse on	B:Discharge Current	C:Dielectric Fluid Pressure	D:Powder Concentration	MRR	Surface Roughness	Residual Stress	Micro Hardness
	µs	Ampere	%	g/l				
1	35	4	0.2	4	1	1	1	1
2	35	4	0.2	4	0.905213	0.25647	0.979335	0.6608245
3	35	4	0.2	4	0.153525	0.323629	0.898424	0.6034874
4	35	8	0.4	6	0	0	0	0
5	35	8	0.4	6	0.181043	0.632192	0.884788	0.5502195
6	35	8	0.4	6	0.60141	0.888662	0.872061	0.5792808
7	35	12	0.6	8	0.830074	0.983318	0.878978	0.9518637
8	35	12	0.6	8	0.91325	0.893793	0.967866	0.6692773
9	35	12	0.6	8	0.834391	0.898814	0.900277	0.6293096
10	292.5	4	0.4	8	0.838638	0.903729	0.890779	0.633349
11	292.5	4	0.4	8	0.842817	0.537537	0.891951	0.4927927
12	292.5	4	0.4	8	0.60141	0.995119	0.858192	0.9057921
13	292.5	8	0.6	4	0.924102	0.910913	0.956762	0.6035696
14	292.5	8	0.6	4	0.848963	0.976297	0.884788	0.7817673
15	292.5	8	0.6	4	0.922579	0.525562	0.927261	0.4913789
16	292.5	12	0.2	6	0.536515	0.913259	0.858192	0.5681949
17	292.5	12	0.2	6	0.85098	0.991808	0.876421	0.899718
18	292.5	12	0.2	6	0.921047	0.917882	0.955477	0.4389339
19	550	4	0.6	6	0.85098	0.454271	0.845601	0.449758
20	550	4	0.6	6	0.568022	0.397972	0.848203	0.4688405
21	550	4	0.6	6	0.549577	0.842966	0.852779	0.5490451
22	550	8	0.2	8	0.792697	0.981582	0.871617	0.9108563
23	550	8	0.2	8	0.927122	0.933377	0.958035	0.6669434
24	550	8	0.2	8	0.868464	0.375722	0.899908	0.2480869
25	550	12	0.4	4	0.543128	0.351126	0.800203	0.3334156
26	550	12	0.4	4	0.536515	0.974508	0.820605	0.9050365
27	550	12	0.4	4	0.928619	1	0.740929	0.9050371

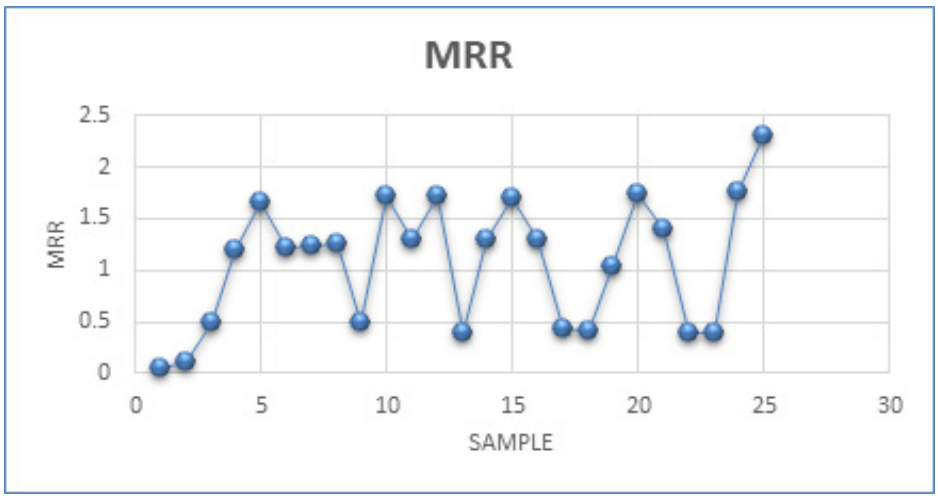

Figure 4. Material removal rate for samples 1-27.

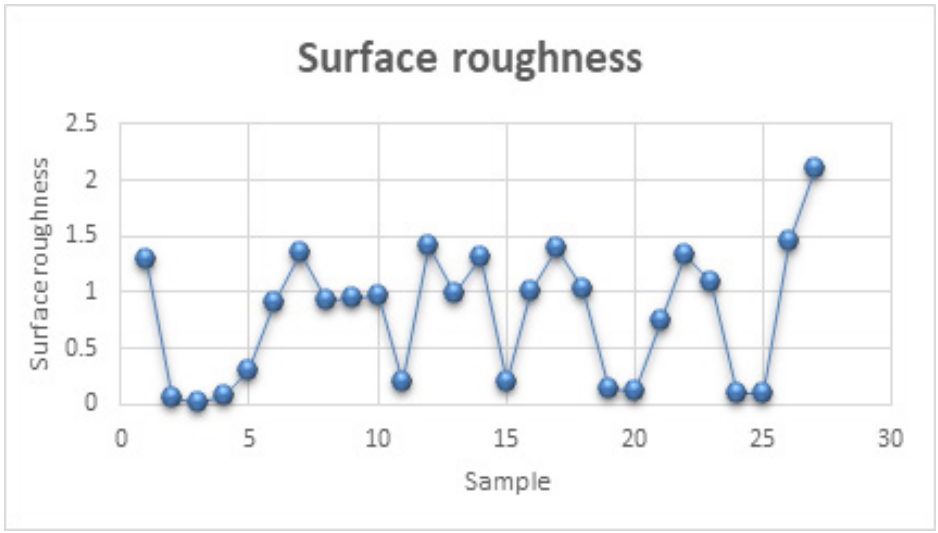

Figure 5. Surface Roughness for samples 1-27.

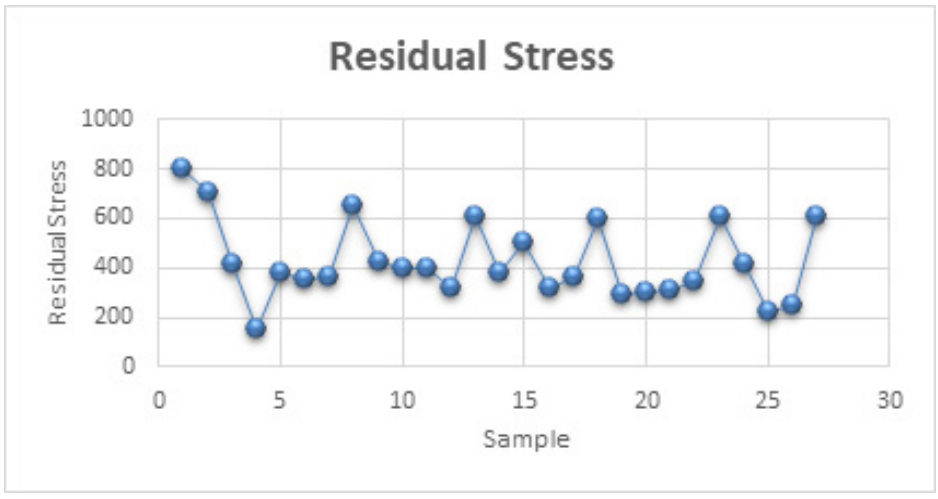

Figure 6. Residual Stress for samples 1-27.

Table 10. The deviation sequences for all experiments

Run	$\Delta_{0i}(1)$	$\Delta_{0i}(2)$	$\Delta_{0i}(3)$	$\Delta_{0i}(4)$
1	0	0	0	0
2	0.094787	0.743529671	0.020665	0.3391755
3	0.846475	0.676370638	0.101576	0.3965126
4	1	1	1	1
5	0.818957	0.367807625	0.115212	0.4497805
6	0.39859	0.111337564	0.127939	0.4207192
7	0.169926	0.016681916	0.121022	0.0481363
8	0.08675	0.106206588	0.032134	0.3307227
9	0.165609	0.101185995	0.099723	0.3706904
10	0.161362	0.096271082	0.109221	0.366651
11	0.157183	0.462463273	0.108049	0.5072073
12	0.39859	0.004880566	0.141808	0.0942079
13	0.075898	0.089087468	0.043238	0.3964304
14	0.151037	0.023703489	0.115212	0.2182327
15	0.077421	0.47443771	0.072739	0.5086211
16	0.463485	0.086741228	0.141808	0.4318051
17	0.14902	0.008192061	0.123579	0.100282
18	0.078953	0.082118412	0.044523	0.5610661
19	0.14902	0.545728787	0.154399	0.550242
20	0.431978	0.602027965	0.151797	0.5311595
21	0.450423	0.157033992	0.147221	0.4509549
22	0.207303	0.018417622	0.128383	0.0891437
23	0.072878	0.066623109	0.041965	0.3330566
24	0.131536	0.624277954	0.100092	0.7519131
25	0.456872	0.648874291	0.199797	0.6665844
26	0.463485	0.025492412	0.179395	0.0949635
27	0.071381	0.00896251	0.259071	0.0949629
ξ	0.8	0.1	0.1	0.9

Table 11. Grey Relational Coefficient for the response

Run	$\Delta_{0i}(1)$	$\Delta_{0i}(2)$	$\Delta_{0i}(3)$	$\Delta_{0i}(4)$
1	1	1	1	1
2	0.880739	0.118549	0.82874	0.2276994
3	0.452642	0.128804	0.496091	0.2014047
4	0.411765	0.090909	0.090909	0.0909091
5	0.460842	0.213763	0.464659	0.1818908
6	0.637181	0.473177	0.438714	0.1920421
7	0.804666	0.857031	0.452443	0.6750542
8	0.889736	0.484951	0.756805	0.2321679
9	0.808679	0.497052	0.500694	0.2124539
10	0.812666	0.509499	0.477963	0.2142929
11	0.816628	0.177789	0.480656	0.1646884
12	0.637181	0.953465	0.41355	0.514912
13	0.902181	0.528856	0.698136	0.2014381
14	0.822526	0.808385	0.464659	0.3142355
15	0.900413	0.174083	0.578907	0.1643058
16	0.601641	0.5355	0.41355	0.1880388
17	0.82448	0.924282	0.447269	0.499296
18	0.898643	0.549093	0.691931	0.1512708
19	0.82448	0.154864	0.393084	0.1537889
20	0.618386	0.142444	0.397145	0.1584385
21	0.608472	0.389054	0.404496	0.1815031
22	0.771517	0.844469	0.437862	0.5286985
23	0.905706	0.600157	0.704401	0.2309167
24	0.841815	0.138069	0.499771	0.1173829
25	0.60508	0.133534	0.33356	0.1304488
26	0.601641	0.796861	0.357916	0.5129166
27	0.907463	1	0.278496	0.5129181

Table 12. Grey Relational Grade and its order

	Factor 1	Factor 2	Factor 3	Factor 4	GRG	Rank
Run	A:Pulse on	B:Discharge Current	C:Dielectric Fluid Pressure	D:Powder Concentration		
	µs	Ampere	%	g/l		
1	35	4	0.2	4	1	1
2	35	4	0.2	4	0.513932	13
3	35	4	0.2	4	0.319736	25
4	35	8	0.4	6	0.171123	27
5	35	8	0.4	6	0.330289	23
6	35	8	0.4	6	0.435278	17
7	35	12	0.6	8	0.697298	2
8	35	12	0.6	8	0.590915	9
9	35	12	0.6	8	0.50472	14
10	292.5	4	0.4	8	0.503605	15
11	292.5	4	0.4	8	0.409941	19
12	292.5	4	0.4	8	0.629777	6
13	292.5	8	0.6	4	0.582653	10
14	292.5	8	0.6	4	0.602451	8
15	292.5	8	0.6	4	0.454427	16
16	292.5	12	0.2	6	0.434683	18
17	292.5	12	0.2	6	0.673832	4
18	292.5	12	0.2	6	0.572734	11
19	550	4	0.6	6	0.381554	22
20	550	4	0.6	6	0.329104	24
21	550	4	0.6	6	0.395881	21
22	550	8	0.2	8	0.645637	5
23	550	8	0.2	8	0.610295	7
24	550	8	0.2	8	0.399259	20
25	550	12	0.4	4	0.300655	26
26	550	12	0.4	4	0.567334	12
27	550	12	0.4	4	0.674719	3

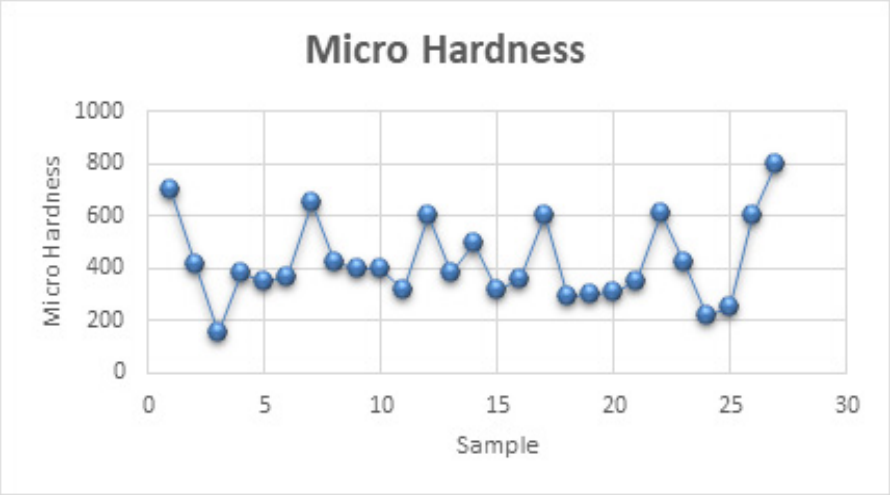

Figure 7. Micro Hardness for samples 1-27.

Grey Relational Coefficient (GRC) was calculated by using Equation (10). The weight of each response (ξ) are taken from Table 10, which is evaluated using the standard deviation objective weighting method and shown in Table 10. Grey Relational Grade (GRG) and ranking were calculated using Equation (11) and shown in Table 12.

6.0 Results and Discussion

6.1 Analysis of MRR

The experiments were carried out with the aim of enhancing the higher erosion rate. Helium and nitrogen were incorporated with metallic powders such as aluminum, graphite, and zinc as a dielectric medium, operating at different pressures. The rationale behind this approach lies in the fact that graphite powder possesses superior thermal conductivity and lower density when compared to aluminum and zinc. This combination with gas assistance (nitrogen, helium) aims to take advantage of the lower density and higher conductivity of graphite, resulting in the formation and dispersion of grain particles in the dielectric medium, thereby improving the erosion rate in machining[21]. From Figure 9, shows the effect of Pulse on time , discharge current , dielectric fluid pressure and powder concentration on material removal. It concluded that an increase in the mist pressure of the dielectric medium leads to a corresponding increase in the Material Removal Rate (MRR). Specifically, when graphite powder is combined with nitrogen gas as the dielectric mixture, a higher MRR is achieved. This heightened MRR can be attributed to the exothermic chemical reaction induced by the combination of nitrogen gas and powders, leading to an oxidation process. On the other hand, the lowest MRR is attained when helium gas is combined with powder as the dielectric medium[22,23]. The preference for nitrogen over helium is explained by the lower ionization energy of nitrogen compared to helium. A gas with lower ionization energy tends to be more ionized, resulting in a higher removal rate (MRR).

The inadequate ionization of helium gas hinders the spark discharge in the machining gap[24]. Figure 8(a,c) illustrates the creation of sizable craters, pores, and cracks on machined samples when nitrogen is introduced along side graphite and zinc powder.

From Figures 8(b,d), it can be seen that pits and micropores are visualized in the machined samples when helium gas is combined with zinc and aluminum powder due to the lower range of MRR. From Figure 8(a), visualized large craters, it means more conductivity and resulted in the generation of spark over the long distance between the gap of machining. It is also observed that higher MRR is achieved at input parameters of pulse duration of 292.5 µs, discharge current of 8 A, dielectric fluid pressure of 0.4 MPa, and powder concentration of 4 g/l when graphite powder, along with nitrogen in the

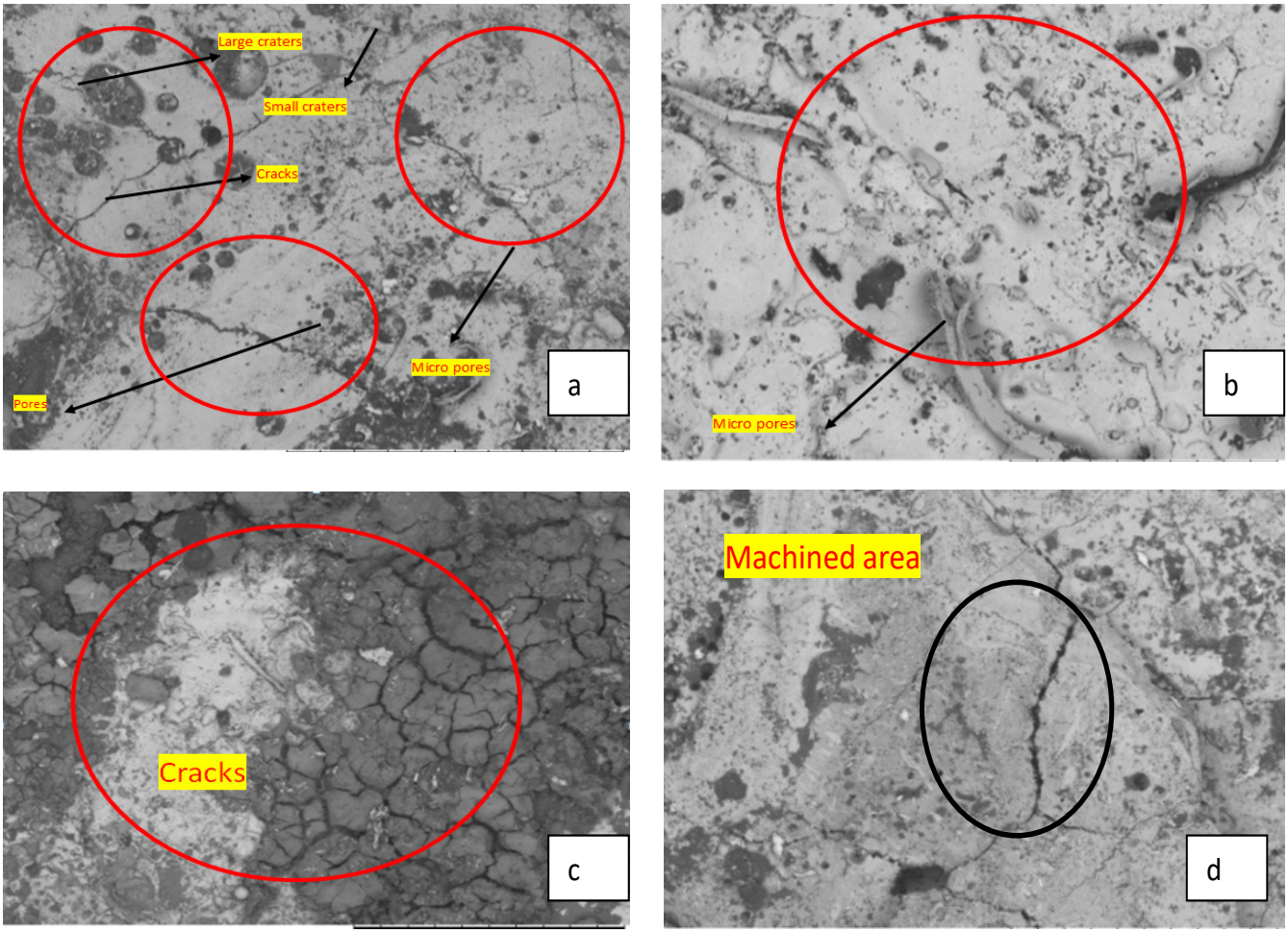

Figure 8. **(a)**. SEM image of machined sample (EN-31) by nitrogen additive with powder of graphite. **(b).** SEM image of sample(EN 31) by helium additive with powder of Aluminium. **(c).** SEM image of machined sample(EN-31) by nitrogen additive with powder of zinc. **(d).** SEM image of machined(EN-31) sample by helium added with powder of zinc.

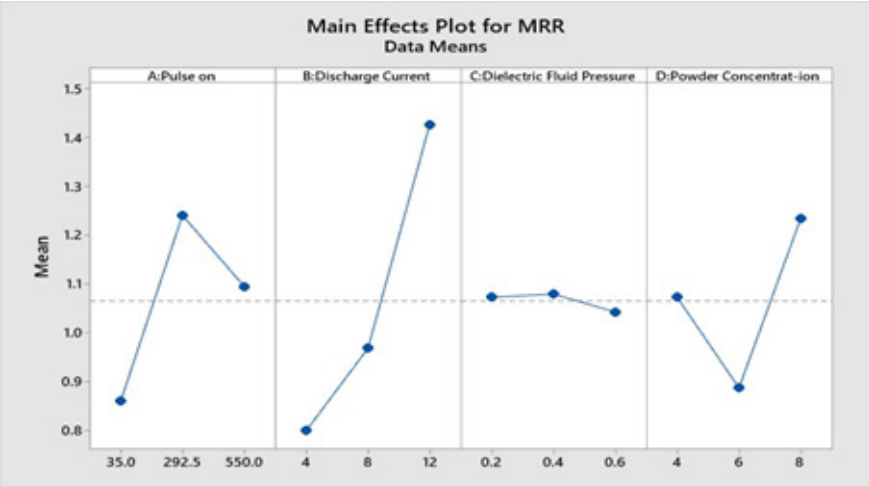

Figure 9. Main effect plot for MRR.

machined samples, forms the largest cavity due to its low density and higher electrical conductivity as compared to helium gas combined with zinc and aluminum powder.

6.2 Surface Roughness

The gas additive method achieves a superior surface finish compared to unconventional electric discharge machining. Figure 11 shows the effect of pulse on time, discharge current, dielectric fluid pressure, and powder concentration on surface roughness. It is also observed that a higher surface finish is achieved at the input parameters of pulse duration of 292.5 µs, discharge current of 8 A, dielectric fluid pressure of 0.4 MPa, and powder concentration of 4 g/l when graphite powder is added to the dielectric medium and mixed with helium gas. The desirable properties of graphite play a crucial role in achieving a high-quality surface finish. Graphite's effective lubrication and low resistivity, in contrast to aluminum and zinc, result in a well-defined microstructure and a more favorable impact on the wetting of powder particles by the molten machine surface[25]. This, in turn, leads to the creation of a smoothly machined surface, as depicted in Figure 10(a).

While aluminum and zinc,combined with a gas additive, yield a satisfactory surface finish, it is not comparable to the performance achieved with graphite powder. Figure 10 (b, c) illustrates the machined sample surfaces using different powders with the addition of helium gas, as also evident in Figure 10 (a). The presence of noble gases in machining contributes to a notably

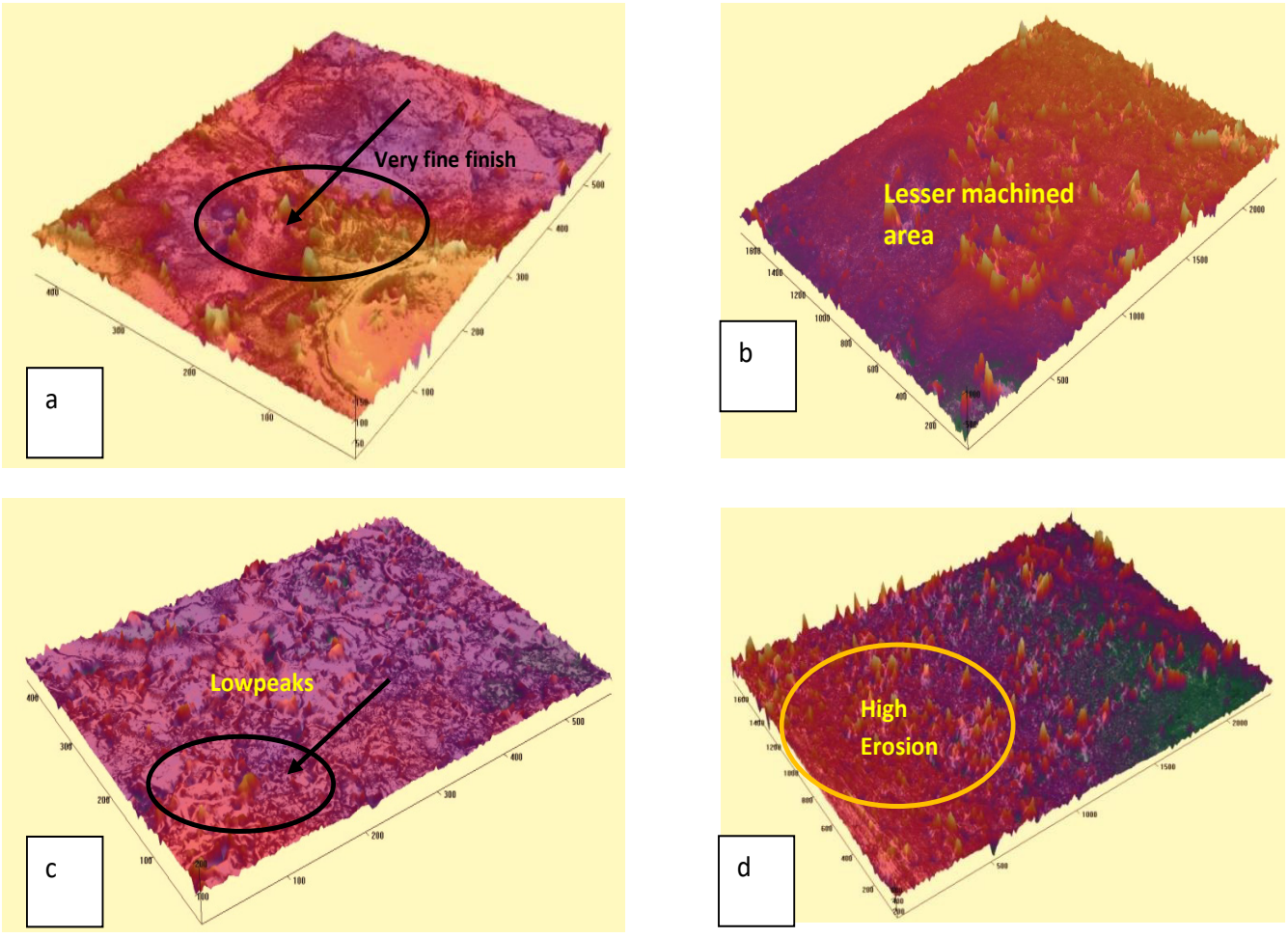

Figure 10. **(a)** profile of Surface with graphite powder additive helium gas. **(b).** profile of surface with Aluminium powder additive helium gas. **(c).** profile of Surface with zinc powder additive helium gas. **(d).** profile of surface with Aluminium powder additive nitrogen gas.

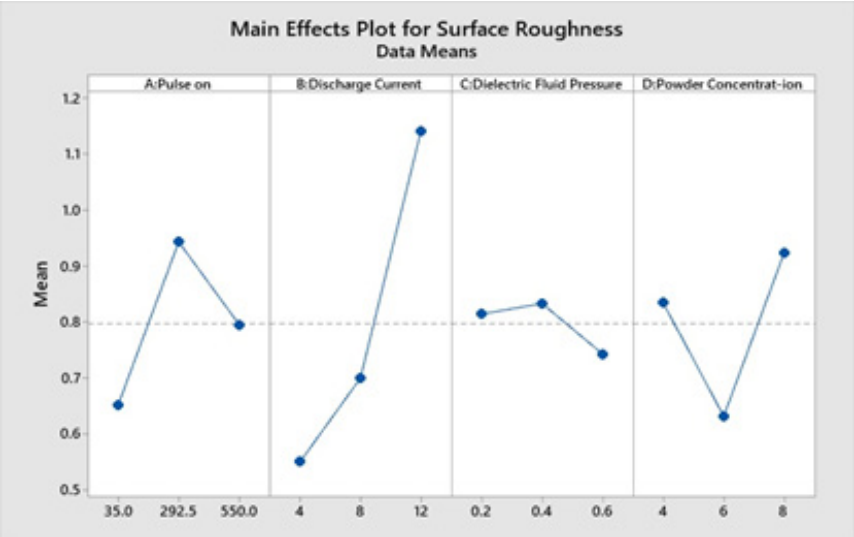

Figure 11. Surface roughness.

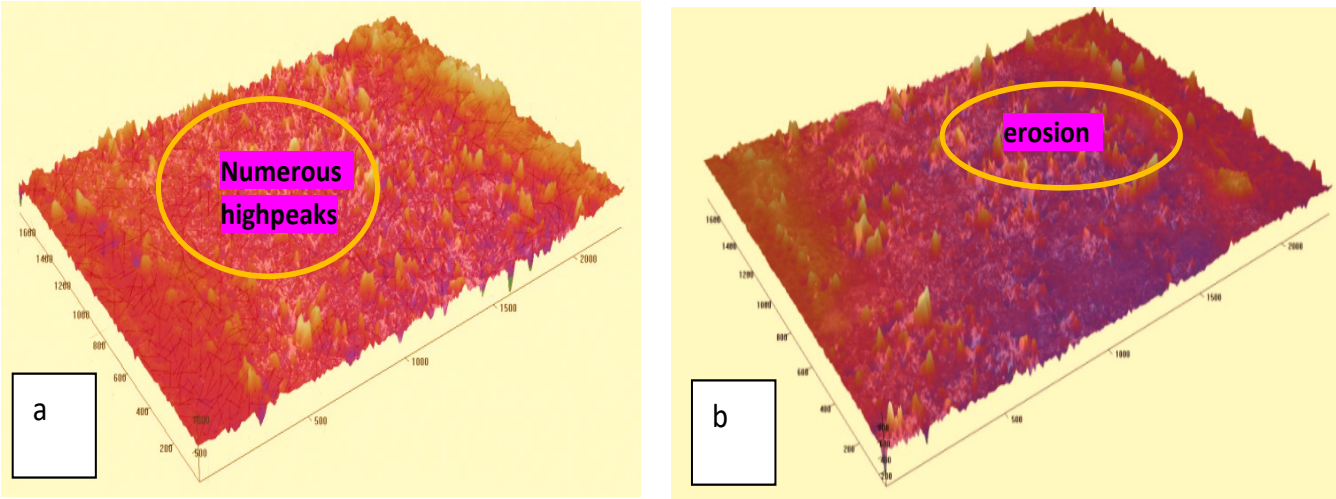

Figure 12. **(a).** profile of surface with graphite powder additive of nitrogen. **(b).** profile of surface with zinc powder additive nitrogen gas.

smoother surface roughness. The reduced oxidation results in stable sparking conditions, leading to a more uniformly distributed arc[26]. The stability of the spark, combined with a larger gap between the workpiece, facilitates a simplified and improved machined-finished surface. Radioscopy images of sample surfaces with various metal powders and the addition of nitrogen gas are presented in Figure 12(a, b).

6.3 Micro-Hardness

The introduction of metal powder into the dielectric (oil and kerosene) enhances the ionization energy effect within the electrode gap. Figure 13 shows the effect of pulse on time, discharge current, dielectric fluid pressure, and powder concentration on microhardness. Which shows an increase in microhardness attributed to the combination of powder additives and gas. The observed pyrolysis effect results in the formation of carbides, contributing to heightened surface hardness by disrupting the carbon and hydrogen bonds[27,28]. In the experimental phase, it is also observed that higher microhardness 821.32 VHN is achieved at the input parameters of pulse

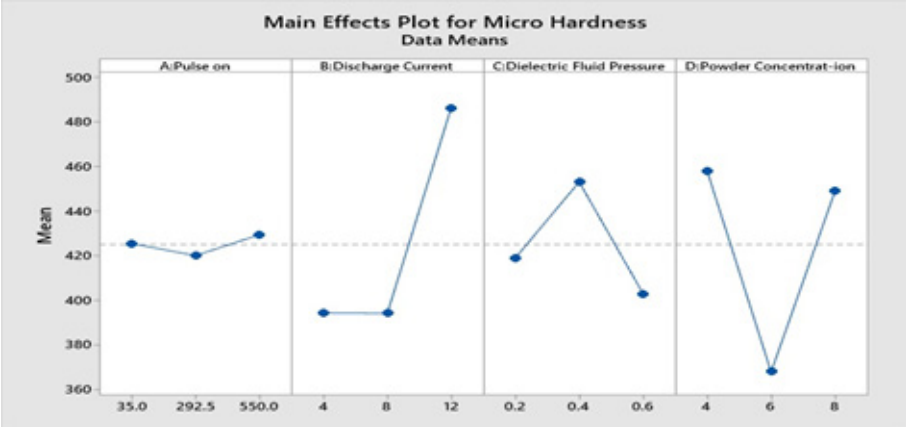

Figure 13. Micro hardness.

duration of 292.5 µs, discharge current of 8 A, dielectric fluid pressure of 0.4 MPa, and powder concentration of 4 g/l when the zinc powder is utilized with the helium gas. In contrast, aluminum powder exhibits a microhardness value of 671.1 VHN, influenced by its lower conductivity. Graphite powder, with a microhardness of 194.13 VHN, is also considered. Among the three powders, zinc stands out with the highest microhardness in near-dry EDM, primarily due to its smaller spark gap. Comparing metallic powders, the dielectric medium enriched with zinc additive attains the highest microhardness, attributed to the smallest spark gap during machining, facilitated by its low electrical conductivity.

6.4 Residual Stress

Figure 15 shows the effect of pulse on time, discharge current, dielectric fluid pressure, and powder concentration on residual stress. It is also observed that a lower residual stress of 229 MPa is achieved at the input parameters of pulse duration of 292.5 µs, discharge current of 8 A, dielectric fluid pressure of 0.4 MPa, and powder concentration of 4 g/l when the utilization of alluminium powder with helium results in lower range of residual stresses compared to other machining processes. In Figure 17(f), the residual stress value is depicted as 229 MPa for the machined EN-31 sample

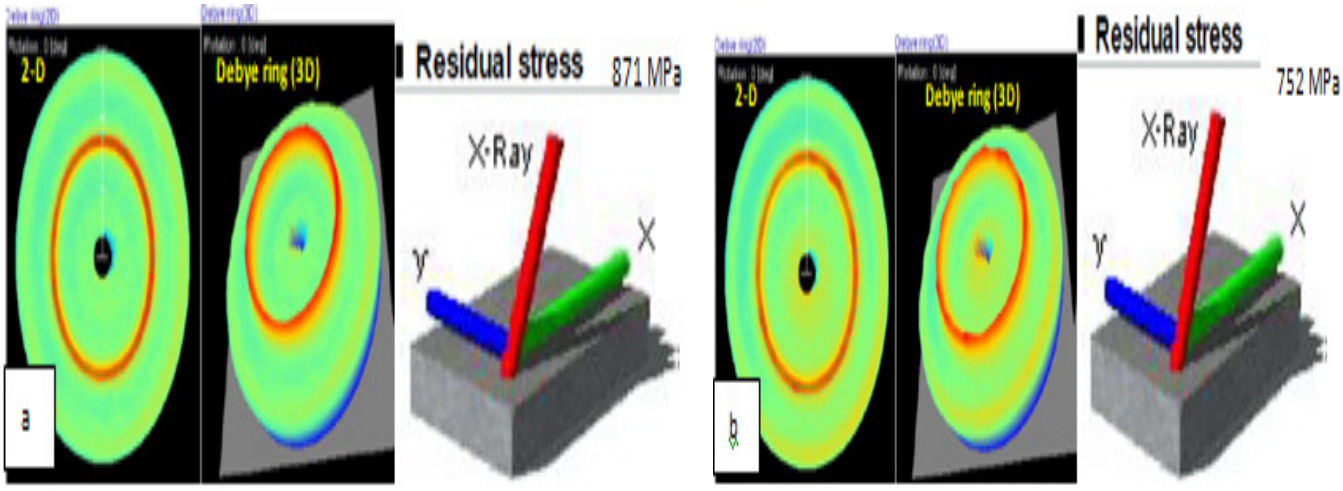

Figure 14. **(a)** Residual stress values machined sample (EN-31) samples by GAP-MND-EDM with graphite and nitrogen. **(b).** Residual stress values of machined sample (EN-31) with GAP-MND-EDM with aluminium and nitrogen.

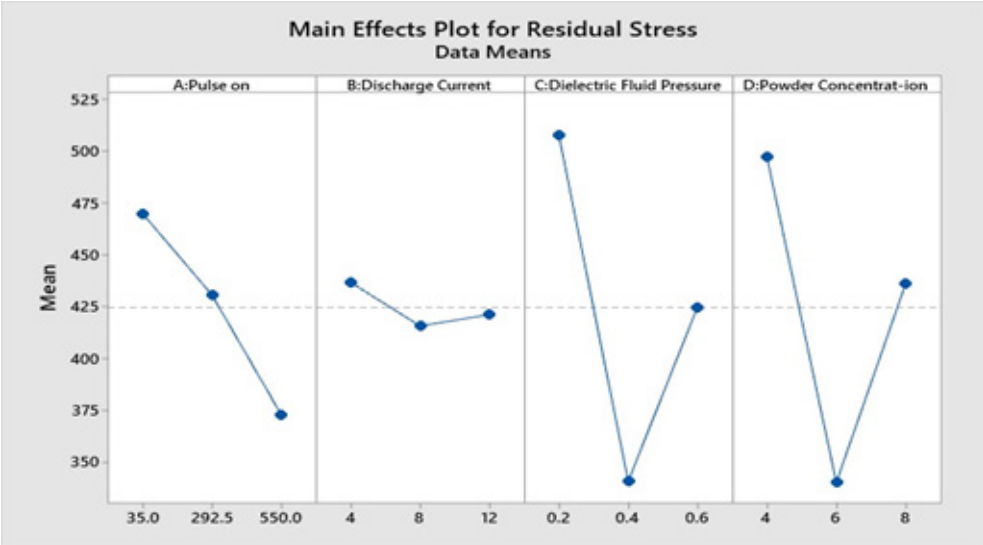

Figure 15. Residual stress.

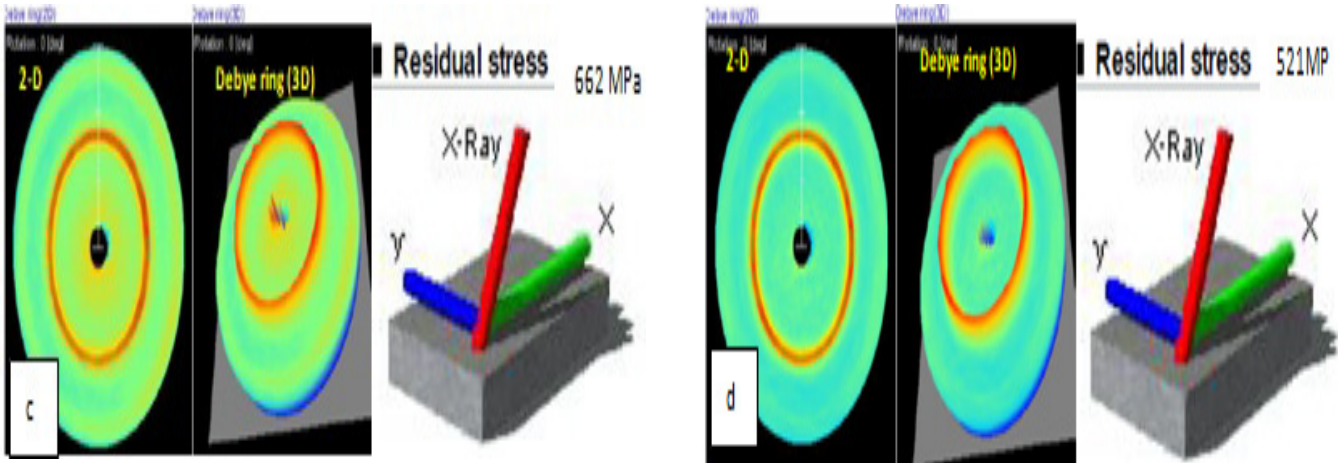

Figure 16. **(c).** Residual stress values of machined sample(EN-31) by GAP-MND-EDM with additive zinc and nitrogen. **(d).** Residual stress values of machined sample (EN-31) with GAP-MND-EDM by additive helium and graphite.

Table 13. Responses for the GRA Grade

Sr. No	PMNED-EDM process parameters	Grey relational grade			Main effect (Max-Min)	Rank	Mean
		Level 1	Level 2	Level 3			
1	Pulse on	0.5070	**0.5404**	0.4782	0.0622	4	0.5085
2	Discharge Current	**0.4981**	0.4701	0.5574	0.0873	3	0.50853
3	Dielectric fluid pressure	**0.5043**	0.5744	0.4469	0.1275	2	0.508533
4	Powder Concentration	**0.4091**	0.5466	0.5699	0.1608	1	0.508533

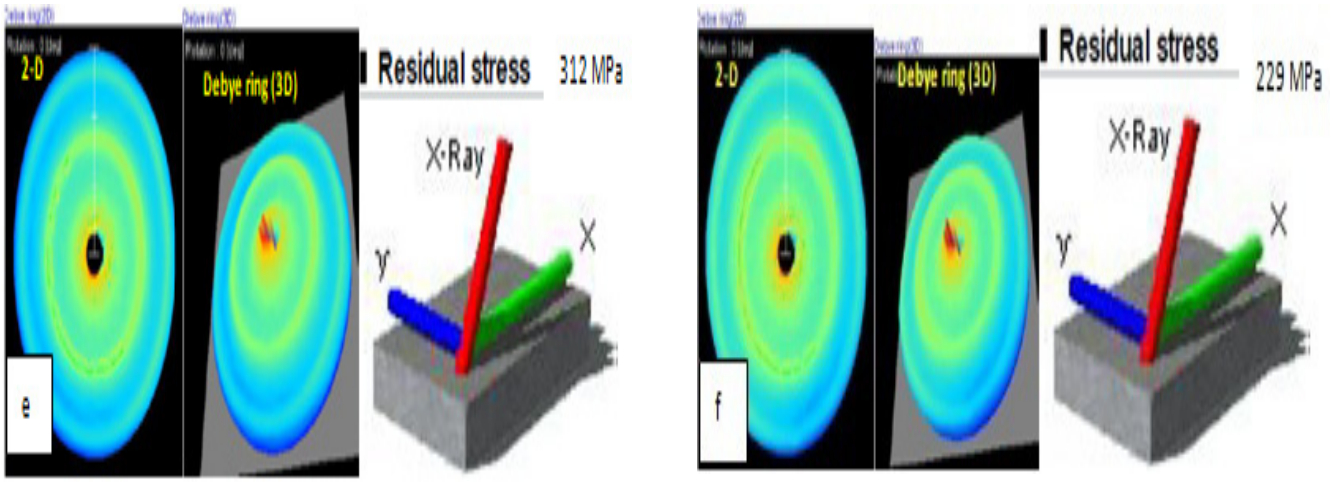

Figure 17. **(e)**. Residual stress values of machined sample(EN-31) with GAP-MND with additive helium and zinc. **(f).** Residual stress values of machined sample (EN-31) by GAP-MND-EDM with additive helium and aluminium powder.

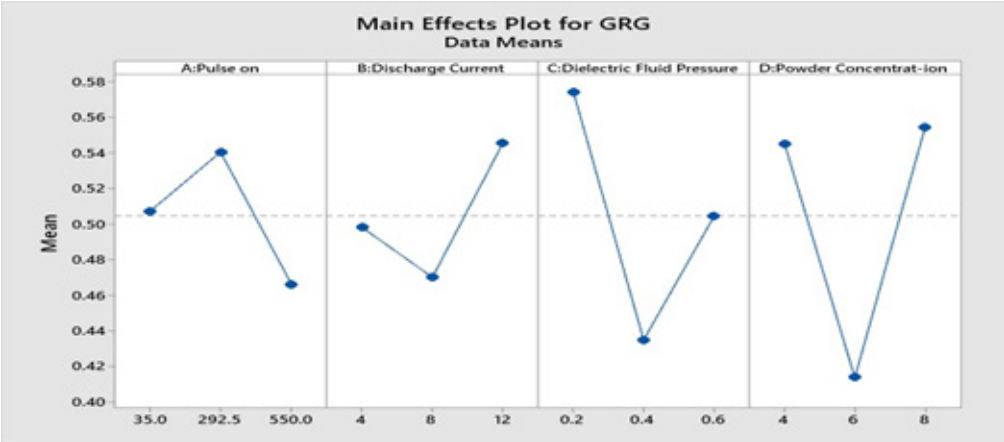

Figure 18. Main effect plot for GRG.

when helium gas is added with alluminium powder in near-dry EDM, measured by Debye Scherer rings. The increased density within the powder-mixed dielectric of non-conventional electrical discharge machines results in a reduction of discharge energy and, consequently, less residual thermal stress. Figures 14(a), (b), 16(c), (d) and 17(e), (f) illustrates the distribution of residual stresses with the depth of the sample with different powders and gases. Additionally, it is noteworthy that effective cooling and flushing are crucial factors in resisting stress-induced stress during the simultaneous occurrence of tension and cooling processes[29].

7.0 Conclusion

The accomplishment of superior results on EN-31 die steel is attributed to the utilization of gas additive powder mixed near dry (EDM). The successful implementation of powder-mixed near-dry EDM was carried out through an orthogonal array design of experiments focused on the selected material. In this study, the standard deviation objective weighting method and grey relational optimization method were employed to enhance multiple responses, including Material Removal Rate (MRR), Surface Roughness (SR), residual stress,

and Microhardness (MH). The optimal combination of parameters, denoted as A2B2C2D1, was identified as the preferred configuration. The key process parameters for gas additive powder mixed near dry-EDM determined through this optimization were a pulse-off duration of 292.5 µs, a discharge current of 8 A, a dielectric fluid pressure of 0.4 MPa, and a powder concentration of 4 g/l. Among these parameters, the pulse off duration holds a prominent role in powder mixed near dry EDM, followed by pulse on time, discharge current, dielectric fluid pressure, and powder concentration. The standard deviation objective weighting method effectively assigned weight fractions for material removal (0.8), surface roughness (0.1), residual stress (0.1), and microhardness (0.9).

8.0 References

1. Zain ZM, Ndaliman MB, Khan AA, Ali MY. Improving micro-hardness of stainless steel through powder-mixed electrical discharge machining. Proceedings of the Institution of Mechanical Engineers, Part C: Journal of Mechanical Engineering Science. 2014; 228(18):3374-80. https://doi.org/10.1177/0954406214530872
2. Wong YS, Lim LC, Rahuman I, Tee WM. Near-mirror-finish phenomenon in EDM using powder-mixed dielectric. Journal of Materials Processing Technology. 1998; 79(1-3):30-40. https://doi.org/10.1016/S0924-0136(97)00450-0
3. Talla G, Gangopadhyay S, Biswas CK. Influence of graphite powder mixed EDM on the surface integrity characteristics of Inconel 625. Particulate Science and Technology. 2017; 35(2):219-26. https://doi.org/10.1080/02726351.2016.1150371
4. Talla G. Powder-Mixed Electric Discharge Machining (PMEDM) of inconel 625 (Doctoral dissertation).
5. Ndaliman MB, Khan AA, Ali MY. Influence of dielectric fluids on surface properties of electrical discharge machined titanium alloy. Proceedings of the Institution of Mechanical Engineers, Part B: Journal of Engineering Manufacture. 2013; 227(9):1310-6. https://doi.org/10.1177/0954405413488592
6. Murali MS, Yeo SH. Process simulation and residual stress estimation of micro-electrodischarge machining using finite element method. Japanese Journal of Applied Physics. 2005; 44(7R):5254. https://doi.org/10.1143/JJAP.44.5254
7. Liqing L, Yingjie S. Study of dry EDM with oxygen-mixed and cryogenic cooling approaches. Procedia Cirp. 2013; 6:344-50. https://doi.org/10.1016/j.procir.2013.03.055
8. Kunleda M, Miyoshi Y, Takaya T, Nakajima N, ZhanBo Y, Yoshida M. High speed 3D milling by dry EDM. CIRP Annals. 2003; 52(1):147-50. https://doi.org/10.1016/S0007-8506(07)60552-6
9. Kunieda M, Yoshida M, Taniguchi N. Electrical discharge machining in gas. CIRP Annals. 1997; 46(1):143-6. https://doi.org/10.1016/S0007-8506(07)60794-X
10. Kung KY, Horng JT, Chiang KT. Material removal rate and electrode wear ratio study on the powder mixed electrical discharge machining of cobalt-bonded tungsten carbide. The International Journal of Advanced Manufacturing Technology. 2009; 40:95-104. https://doi.org/10.1007/s00170-007-1307-2
11. Khundrakpam NS, Brar GS, Deepak D, Nanak G. A comparative study on machining performance of wet EDM, near dry EDM and powder mixed near dry EDM. Int J Appl Eng Res. 2018; 13(11):9378-81.
12. Kansal HK, Singh S, Kumar P. Parametric optimization of powder mixed electrical discharge machining by response surface methodology. Journal of Materials Processing Technology. 2005; 169(3):427-36. https://doi.org/10.1016/j.jmatprotec.2005.03.028
13. Chow HM, Yan BH, Huang FY, Hung JC. Study of added powder in kerosene for the micro-slit machining of titanium alloy using electro-discharge machining. Journal of Materials Processing Technology. 2000; 101(1-3):95-103. https://doi.org/10.1016/S0924-0136(99)00458-6
14. Bai X, Zhang QH, Li TT, Zhang JH. Powder mixed near dry electrical discharge machining. Advanced Materials Research. 2012; 500:253-8. https://doi.org/10.4028/www.scientific.net/AMR.500.253
15. Bai X, Zhang QH, Yang TY, Zhang JH, Tan J. Research on tool wear rate of powder mixed near dry electrical discharge machining. Advanced Materials Research. 2013; 652:2222-7. https://doi.org/10.4028/www.scientific.net/AMR.652-654.2222
16. Tripathy S, Tripathy DK. Optimization of process parameters and investigation on surface characteristics during EDM and powder mixed EDM. InInnovative Design and Development Practices in Aerospace and Automotive Engineering: I-DAD, February 22-24, 2016. Springer Singapore. 2017; 385-91. https://doi.org/10.1007/978-981-10-1771-1_41

17. Tsai HC, Yan BH, Huang FY. EDM performance of Cr/Cu-based composite electrodes. International Journal of Machine Tools and Manufacture. 2003; 43(3):245-52. https://doi.org/10.1016/S0890-6955(02)00238-9
18. Tzeng YF, Lee CY. Effects of powder characteristics on electrodischarge machining efficiency. The International Journal of Advanced Manufacturing Technology. 2001; 17:586-92. https://doi.org/10.1007/s001700170142
19. Upadhyay L, Aggrawal ML, Pandey PM. Performance analysis of magnetorheological fluid-assisted electrical discharge machining. Materials and Manufacturing Processes. 2018; 33(11):1205-13. https://doi.org/10.1080/10426914.2017.1364852
20. Van Dijck FS, Dutre WL. Heat conduction model for the calculation of the volume of molten metal in electric discharges. Journal of Physics D: Applied Physics. 1974; 7(6):899. https://doi.org/10.1088/0022-3727/7/6/316
21. Vignesh M, Ramanujam R. Laser-assisted high speed machining of Inconel 718 alloy. High Speed Machining. Academic Press. 2020; 243-62. https://doi.org/10.1016/B978-0-12-815020-7.00009-6
22. Astakhov VP. Tribology of metal cutting. Mechanical Tribology, New York: Marcel Dekker; 2004. p. 307-46.
23. Rao PS, Ramji K, Satyanarayana B. Effect of wire EDM conditions on generation of residual stresses in machining of aluminum 2014 T6 alloy. Alexandria Engineering Journal. 2016; 55(2):1077-84. https://doi.org/10.1016/j.aej.2016.03.014
24. Singh M. The ally must die: Theorizing a politics of death and unbodiment. Sikh Formations. 2023; 1-5. https://doi.org/10.1080/17448727.2023.2289289
25. Singh NK, Sethuraman B. Development and characterization of Aluminium AA7075 Hybrid Composite Foams (AHCFs) using SiC and TiB2 Reinforcement. International Journal of Metalcasting. 2023; 1-6. https://doi.org/10.21203/rs.3.rs-1718478/v1
26. Singh NK, Pradhan SK. Experimental and numerical investigations of pipe orbital welding process. Materials Today: Proceedings. 2020; 27:2964-9. https://doi.org/10.1016/j.matpr.2020.04.902
27. Rathore RK, Awasthy M, Himte R, Shukla AK, Kanoje N, Singh NK. Response surface optimized robotic spray-painting metamodeling for fanuc paint Robot P-250IB/15.
28. Singh NK, Balaguru S. Experimental analysis of foaming agent contents in AA7075/SiC closed cell aluminum composite foam. International Conference on Sustainable Technologies and Advances in Automation, Aerospace and Robotics. Singapore: Springer Nature Singapore. 2022; 567-75. https://doi.org/10.1007/978-981-99-2349-6_51
29. Rathore RK, Singh NK, Xavier JF. Characterization of AA7075 alloy foam using calcium and magnesium carbonate as foaming agent. Processing and Characterization of Materials: Select Proceedings of CPCM 2020. 2021; 289-97. https://doi.org/10.1007/978-981-16-3937-1_30